Presented at the 1979 Society of Petroleum Engineers of AIME 5th Symposium on Reservoir Simulation, Denver, Colorado, February 1-2, 1979

LBL-8802

CONF-790119--2

Jan. 31

DESCRIPTION OF THE THREE-DIMENSIONAL TWO-PHASE SIMULATOR SHAFT78 FOR USE IN GEOTHERMAL RESERVOIR STUDIES

Karsten Pruess, J. Mike Zerzan,
Ron C. Schroeder, and Paul A. Witherspoon

January 1979

Prepared for the U. S. Department of Energy
under Contract W-7405-ENG-48

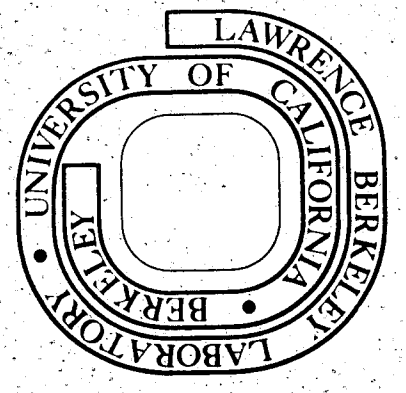

DISCLAIMER

DESCRIPTION OF THE THREE-DIMENSIONAL TWO-PHASE SIMULATOR SHAFT78 FOR USE IN GEOTHERMAL RESERVOIR STUDIES

by Karsten Pruess, J. Mike Zerzan, and Ron C. Schroeder, Paul A. Witherspoon, Members SPE-AIME, Lawrence Berkeley Lab.

ABSTRACT

The algorithm of SHAFT78 is based on mass and energy-balance equations for two-phase flow in a porous medium. We convert the basic differential equations into integrated finite-difference form. This allows regular and irregular reservoir shapes to be handled with the same ease. The equations are solved semi-implicitly for discrete time steps. The present version of SHAFT78 treats the coupling between mass and energy flow in a noniterative way. Special provisions are made to compute phase transitions with high accuracy.

We have verified the program by computing a number of sample problems that previously had been investigated by other authors. Our model studies reveal that two-phase geothermal reservoirs are capable of a great variety of pressure responses upon production. We show that the standard technique of estimating reserves by extrapolating a plot of p/Z vs cumulative production is not applicable to two-phase geothermal reservoirs. We develop a bulk model (lumped parameters) for a two-phase reservoir that admits an analytical solution for pressure decline upon production. From this we conclude that in many cases pressure will be a linear function of cumulative production, with the slope allowing an estimate of total reservoir volume. Reserve assessment requires knowledge of average porosity and vapor saturation, which cannot be obtained from pressure decline curves.

INTRODUCTION

Geothermal reservoirs are distinguished by the fact that, in contrast to oil and gas reservoirs, fluid flow, in general, is not isothermal. The processes of water boiling and steam condensation involve exchange of large quantities of heat between the fluid and the rock matrix. The flow of steam and water alters both the distribution of mass and energy in the reservoir.[1] A theoretical description of two-phase geothermal reservoirs, then, must consider both mass and energy transport.[2]

In recent years, a number of numerical simulators for geothermal reservoirs have been developed.[3-10] The general purpose of these is to aid reservoir engineers in (1) determining characteristic parameters of reservoirs (most important among those being the reserves of fluid and heat) and (2) simulating the performance of reservoirs upon production and injection.

The various simulators differ in the approximations made in the underlying physical model (e.g., dependence of rock and fluid properties on thermodynamic variables), in the geometrical definition of the reservoir (one-, two-, or three-dimensional, regular or irregular shape), in the choice of thermodynamic variables, and in the mathematical techniques used for solving the coupled mass and energy transport equations.

Criteria for desirable performance of numerical simulators depend in part on the particular problems to be investigated. Different problems often will differ in the required level of detail to be resolved, and in the optimum balance of speed and accuracy of computation. Much can be learned about two-phase flow in porous media from model studies for idealized systems. Such studies can be performed with less-than-three-dimensional models and algorithms that are based on regular grid spacings. For modeling natural geothermal reservoirs, on the other hand, it is important that irregular three-dimensional geometries may be handled easily.

In comparison with other two-phase simulators that have been discussed in the literature, the main distinctive feature of SHAFT78 is that it uses an integrated finite-difference method (IFD).[11] We solve finite-difference equations that are obtained by formally integrating the basic partial differential equations for mass and energy flow over arbitrary polyhedral volume elements. This method is as easily applicable to irregular geometries of actual reservoirs as it is to idealized regular geometries; yet the relative simplicity of the finite-difference method is retained in the theory and algorithms.

References and illustrations at end of paper.

E&G

Another advantage of SHAFT78 is that all fluid properties are obtained through interpolation from tables.[12] No reference to the equation of state of water is built into the algorithm, which therefore also can be applied for studying two-phase porous flow of fluids other than water.

The version of SHAFT78 discussed in Chapters 1 and 2 of this paper is not to be considered final. Future development will allow rock properties to vary with temperature and pressure, such variations being neglected at present. Also, we intend to implement an iterative solution of the coupled mass and energy transport equations in order to overcome limitations of time step size inherent in our present noniterative treatment of the coupling.

The present version of SHAFT78, however, is fully operative and is being used extensively. In Chapter 3, we discuss results of calculations for idealized systems, which verify the program and give insight into the pressure response of two-phase reservoirs during production.

Simulations of "real" reservoirs also have been carried out.[13] Work on simulating reinjection into the highly irregular-shaped geothermal field near Serrazzano (Italy) is in progress.[14]

1. PHYSICAL AND MATHEMATICAL MODEL

Mass and Energy Balances

Following the customary procedure, we describe the flow of (two-phase) fluid and heat in a porous medium in terms of balance equations for mass and energy. We have the density equation,

$$\frac{\partial \phi \rho}{\partial t} = - \operatorname{div} \underset{\sim}{F} + q, \quad \ldots\ldots\ldots\ldots (1)$$

and the energy equation,

$$\frac{\partial (\text{energy/volume})}{\partial t} = - \operatorname{div} \underset{\sim}{G} + \left(\frac{\underset{\sim}{F}_v}{\rho_v} + \frac{\underset{\sim}{F}_\ell}{\rho_\ell}\right) \nabla p + Q . \quad \ldots\ldots\ldots\ldots\ldots\ldots (2)$$

The momentum balance is approximated with Darcy's law[15]

$$\underset{\sim}{F} = \sum_{\alpha=v,\ell} \underset{\sim}{F}_\alpha = - \sum_\alpha \frac{k\, k_\alpha}{\mu_\alpha} \rho_\alpha (\nabla p - \rho_\alpha \underset{\sim}{g}) . \quad \ldots\ldots\ldots\ldots\ldots\ldots (3)$$

The energy flux $\underset{\sim}{G}$ is taken to be the sum of conductive heat fluxes in rock and fluid, plus the enthalpy fluxes of vapor and liquid:

$$\underset{\sim}{G} = - K \nabla T + \sum_{\alpha=v,\ell} \underset{\sim}{F}_\alpha h_\alpha . \quad \ldots\ldots\ldots\ldots (4)$$

Eqs. 2 and 4 are straightforward statements of the first law of thermodynamics, with viscous dissipation being neglected. Other approximations made in defining the physical model are: (1) we assume all rock properties—porosity, density, specific heat, thermal conductivity, absolute permeability—to be independent of temperature, pressure, or vapor saturation; (2) we neglect capillary pressure $p_c = p_\ell - p_v$; (3) we assume that liquid, vapor, and rock matrix are in local thermodynamic equilibrium, i.e., at the same temperature and pressure, at all times; (4) we neglect the $(F/\rho)\nabla p$ - terms in Eq. 2.

With liquid and vapor in thermodynamic equilibrium, the state of the two-phase fluid can be specified completely in terms of specific energy, u, and specific density, ρ. For the rock/fluid mixture we have

$$\frac{\text{energy}}{\text{volume}} = \phi u \rho + (1-\phi)\, u_R\, \rho_R . \quad \ldots\ldots\ldots\ldots (5)$$

Because of thermodynamic equilibrium, the specific energy, u_R, of the rock is a function of fluid temperature, T, which in turn is a function of (u,ρ):

$$\frac{\partial u_R}{\partial t} = \left(\frac{\partial u_R}{\partial u}\right)_\rho \frac{\partial u}{\partial t} + \left(\frac{\partial u_R}{\partial \rho}\right)_u \frac{\partial \rho}{\partial t} \quad \ldots\ldots\ldots\ldots (6)$$

with Eqs. 5, 6, 1 and the above stated approximations Eq. 2 can be written

$$\frac{\partial u}{\partial t}\left[\phi \rho + (1-\phi)\, \rho_R \left\{\left(\frac{\partial u_R}{\partial u}\right)_\rho + \left(\frac{\partial u_R}{\partial \rho}\right)_u \frac{\partial \rho / \partial t}{\partial u / \partial t}\right\}\right]$$

$$= - \operatorname{div} \underset{\sim}{G} + u \operatorname{div} \underset{\sim}{F} + (Q - uq) . \quad \ldots\ldots\ldots\ldots (7)$$

For the solution of Eqs. 1 and 7, different sets of variables can be used. The formally most elegant choice is (u,ρ), which also appears to be advantageous with regard to ensuring over-all mass and energy conservation. This is the method adopted in the present work. A difficulty associated with the (u,ρ)-formulation is that liquid subcooled water has a very small compressibility. Very small density changes translate into large variations in pressure. Extreme accuracy is required in computing liquid densities in order to get reliable values for the flow terms (Eqs. 3 and 4). For this reason, alternative sets of variables such as pressure and enthalpy may be preferable for problems involving liquid subcooled water.

Integrated Finite-Difference Method

In order to be able to handle one-, two- or three-dimensional, regular or irregular geometries with the same ease, we rewrite Eqs. 1 and 7 in integrated form. The reservoir volume, V, is broken up into a number of arbitrary elementary polyhedrons, V_n, V_m, V_ℓ, . . . , which are connected by polygonal interfaces with area A_{nm}, $A_{n\ell}$, . . . The interfaces between elements must be perpendicular to the line connecting their centers (see Fig. 1). Integrating Eq. 1 gives

$$\phi_n \frac{\partial}{\partial t} \int_{V_n} d\tau\, \rho = \phi_n V_n \frac{\partial \rho_n}{\partial t} = \int_{(V_n)} da\, \underset{\sim}{F} \cdot \underset{\sim}{n} + V_n q_n$$

$$= \sum_m A_{nm} F_{nm} + V_n q_n . \quad \ldots (8)$$

Here we have introduced volume and surface averages. (Note that these are averages of macroscopic quantities and should not be confused with microscopic averaging used to derive the differential Eqs. 1 and 2.) Note that in contrast to the usual convention, we take $\underset{\sim}{n}$ to be the inward normal (into V_n) for surface element da. The sum over m extends over all elements V_m that have an interface A_{nm} in common with V_n. Proceeding with Eq. 7 in an analogous way,

we obtain the integrated density and energy equations for elementary volume, V_n,

$$\frac{\partial \rho_n}{\partial t} = \frac{\sum_m A_{nm} F_{nm}}{\phi_n V_n} + \frac{q_n}{\phi_n} \quad \ldots\ldots\ldots (9)$$

$$\frac{\partial u_n}{\partial t} = \frac{\sum_m A_{nm}(G_{nm} - u_n F_{nm}) + V_n(Q_n - u_n q_n)}{V_n \phi_n \rho_n + V_n(1-\phi_n)\rho_R \left\{\left(\frac{\partial u_R}{\partial u}\right)_\rho + \left(\frac{\partial u_R}{\partial \rho}\right)_u \frac{\partial \rho/\partial t}{\partial u/\partial t}\right\}_n} \quad \ldots\ldots\ldots (10)$$

The flux terms F_{nm} and G_{nm} are computed from the finite-difference forms of Eqs. 3 and 4.

$$(F_\alpha)_{nm} = k_{nm}\left(\frac{k_\alpha}{\mu_\alpha}\right)_{nm} (\rho_\alpha)_{nm}\left[\frac{P_m - P_n}{d_n + d_m} - (\rho_\alpha)_{nm} g_{nm}\right] \quad \ldots\ldots\ldots (11)$$

$$G_{nm} = K_{nm}\frac{T_m - T_n}{d_n + d_m} + \sum_\alpha (F_\alpha)_{nm}(h_\alpha)_{nm}, \quad \ldots\ldots\ldots (12)$$

In order to define completely our mathematical model, we need to complement Eqs. 9 through 12 with prescriptions for computing interface quantities from volume averages. Demanding continuity for conductive heat flux gives

$$K_{nm} = \frac{d_n + d_m}{\frac{d_n}{K_n} + \frac{d_m}{K_m}}, \quad \ldots\ldots\ldots (13)$$

where thermal conductivities may take a jump at the interface, and in general, $K_n \neq K_m$.

An analogous equation holds for the absolute permeability at the interface, if we demand continuity of mass flux

$$k_{nm} = \frac{d_n + d_m}{\frac{d_n}{k_n} + \frac{d_m}{k_m}}, \quad \ldots\ldots\ldots (14)$$

where again k may take a finite jump at the interface, $k_n \neq k_m$. To derive Eqs. 13 and 14, we have assumed that temperature and pressure are continuous at the interface.

The fluid density at the interface is interpolated spatially from that of the adjacent elements:

$$\rho_{nm} = \frac{d_m \rho_n + d_n \rho_m}{d_n + d_m}, \quad \ldots\ldots\ldots (15)$$

Energies and mobilities at interfaces are weighted toward those of the upstream element:

$$u_{nm} = \lambda u_{up} + (1-\lambda) u_{down} \quad \ldots\ldots (16)$$

$$(k_\alpha/\mu_\alpha)_{nm} = \kappa(k_\alpha/\mu_\alpha)_{up} + (1-\kappa)(k_\alpha/\mu_\alpha)_{down} \quad \ldots\ldots\ldots (17)$$

The values to be chosen for the weighting parameters λ and κ depend on the problem studied. Typically, we take $\lambda = 2/3$; $\kappa = 1$ is required for problems involving sharp phase fronts.

We want to emphasize again the main advantages of using an integrated finite-difference method. Namely, all computations are done directly from a list of interfaces A_{nm}, distances d_n, d_m, and element volumes V_n, V_m. There is no reference to the dimensionality of the problem except in the numerical values assigned to the A_{nm}, d_n, d_m, V_n, and V_m. This scheme handles irregular geometries such as occur in actual reservoirs as easily as idealized regular geometries. Elements and interfaces can be modified, appended, or deleted as desired without affecting unmodified parts of the system. Also, volumes, interface areas, and distances can be assigned "artificial" values that do not correspond to any possible geometry in real space in order to model special effects, e.g., boundary conditions. For example, assigning a very large value to the volume of an element will ensure that the element always will remain at (almost) the same temperature, pressure, and vapor saturation.

2. SOLUTION METHOD

Time Discretization

To solve Eqs. 9 and 10, we discretize time as a first-order forward finite difference,

$$\Delta\rho_n = \Delta t \frac{\sum_m A_{nm} \bar{F}_{nm}}{\phi_n V_n} + \frac{\bar{q}_n}{\phi_n}, \quad \ldots\ldots\ldots (18)$$

and expand the time average $\bar{F}_{nm}$ to first order,

$$\bar{F}_{nm} = F_{nm}(t^k + \theta\Delta t) \approx F_{nm}(t^k) + \theta\Delta t \frac{\partial F_{nm}}{\partial t} \approx F_{nm}(t^k) + \theta\left[\left(\frac{\partial F_{nm}}{\partial \rho_n}\right)\Delta\rho_n + \left(\frac{\partial F_{nm}}{\partial \rho_m}\right)\Delta\rho_m\right], \quad \ldots\ldots\ldots (19)$$

where θ is a parameter between 0 and 1, to be discussed below, and k is the time-step index. With Eq. 19 we can rewrite Eq. 18 as

$$\Delta\rho_n = (\Delta\rho_n)_{exp} + \theta(\Delta\rho_n)_{imp}, \quad \ldots\ldots (20)$$

where exp refers to time t^k, and imp refers to time $t^k + \theta\Delta t$. (Note that $t^k + \theta\Delta t \rightarrow t^k + \Delta t = t^{k+1}$ as $\theta \rightarrow 1$.) The explicit part of $\Delta\rho_n$ can be computed from quantities known at the beginning of a time step. The implicit part depends on the changes occurring during Δt. The solution algorithm computes $(\Delta\rho_n)_{exp}$ first, and then uses these values as zero-order approximation in an iterative scheme to compute the full $\Delta\rho_n$.[16,17] A similar approach is

taken for the time-discretization and mixed explicit-implicit solution of the energy equation (Eq. 10).

An overview of the solution procedure employed in SHAFT78 is given in Fig. 2. We first solve the energy equation for a time step Δt_u. Then the density equation is solved for a time step $\Delta t_\rho \leq \Delta t_u$. Often the rate of (relative) energy change is considerably smaller than that of (relative) density change, and SHAFT78 takes longer energy time steps, requiring a number of density steps per energy step. After the density step, a correction to the rock/fluid equilibration is performed (see below). If the correction cannot be done with a preset accuracy, the density step is repeated with half the time step. After an accepted density step, the program either proceeds to the next density step (if the total time $\Sigma \Delta t_\rho$ of all density steps is less than the energy time step Δt_u), or begins another energy step (if $\Sigma \Delta t_\rho = \Delta t_u$).

We have not yet performed a detailed stability analysis of the solution algorithm used in SHAFT78. Note that for every time step the basic nonlinear Eqs. 9 and 10 are replaced with linearized equations with constant coefficients (Eqs. 18, 19, and analogous for the energy equation). These are stable with respect to large time steps for $\Theta > 0.5$.[18] The rock/fluid equilibration introduces a damping of energy changes, which should enhance stability. Thus it appears that stability is not so much a problem as accuracy. In order for the linearized equations to be good approximations, we need "good" values for the derivatives $(\partial F_{nm}/\partial \rho_n)$, etc. SHAFT78 estimates "expected" density and energy changes by extrapolating from time t^k to t^{k+1} and computes the derivatives $(\partial F_{nm}/\partial \rho_n)$, etc., as averages over expected changes. This method obviously will be accurate only for not "too large" time steps, with what is too large depending on the particular problem. In order to accommodate larger time steps, we presently are investigating a fully iterative approach, in which the energy and density-equations will be solved repeatedly for a time step until expected and computed energy and density changes agree to within narrow limits.

Equilibration Between Rock and Fluid

For geothermal problems, the energy and density equations are coupled in two distinct ways, namely, across elements and within elements. The coupling across elements arises because pressure gradients, which in turn drive mass and energy flow, depend on both fluid energy and density. Therefore, a change in fluid density modifies the flow of energy (and vice versa). This coupling is usually not very strong. It presently is treated in SHAFT78 by solving uncoupled energy and density equations in each time step, but limiting the maximum permissible changes in important variables (such as pressure, temperature, and vapor saturation) to a small percentage (1% default).

The coupling between energy and density equations within elements is very strong. It arises from the presence of the rock matrix in thermal equilibrium with the fluid and from the fact that fluid temperature depends on both energy and density. In Eq. 10 this coupling is represented by the term

$$R_n = \frac{\partial \rho_n / \partial t}{\partial u_n / \partial t} \quad , \quad \ldots\ldots\ldots\ldots\ldots \quad (21)$$

i.e., the ratio of density to energy change. This term is needed to solve the energy equation, but it is known only after both energy and density equations are solved in a completely self-consistent way. The present version of SHAFT78 does not solve iteratively the energy and density equations until self-consistency is achieved. Our simpler method consists of making a good guess for R_n at the beginning of a time step, and then correcting for inaccuracies after the energy and density equations have been solved.

Generally speaking, we take as our estimate for R_n the value computed for element n in the last time step, t^k. Occasionally, for a nearly isothermal situation, this will lead to substantial cancellations between the large rock terms in the denominator of Eq. 10, giving rise to numerical inaccuracy. SHAFT78 checks for cancellation effects, and if they are significant, it replaces the extrapolated value of R_n with the isothermal limit,

$$R_n^{\text{isothermal}} = - \frac{(\partial u_R / \partial u_n)_{\rho_n}}{(\partial u_R / \partial \rho_n)_{u_n}} \quad , \quad \ldots\ldots \quad (22)$$

corresponding to $\partial u_R / \partial t = 0$ (cf. Eq. 6). The isothermal limit is also used for the initialization of a simulation.

After the energy step, then, rock and fluid are equilibrated at a temperature

$$T_i = T(u_n + \Delta u_n, \rho_n + R_n \cdot \Delta u_n).$$

However, the subsequent density step usually will yield a density change $\Delta \rho_n \neq R_n \cdot \Delta u_n$, leaving the fluid at the somewhat different temperature $T_f = T(u_n + \Delta u_n, \rho_n + \Delta \rho_n)$. Equilibrating rock and fluid will leave both at the temperature $T(u_n + \Delta u_n', \rho_n + \Delta \rho_n)$. During equilibration, the energy per volume remains constant, from which condition the correction to the energy transfer between rock and fluid can be computed:

$$\frac{\text{energy}}{\text{volume}} = \phi(u_n + \Delta u_n)(\rho_n + \Delta \rho_n) + (1-\phi) u_R(u_n + \Delta u_n, \rho_n + R_n \Delta u_n) * \rho_R$$

(before equilibration)

$$= \phi(u_n + \Delta u_n')(\rho_n + \Delta \rho_n) + (1-\phi) u_R(u_n + \Delta u_n', \rho_n + \Delta \rho_n) * \rho_R$$

(after equilibration) $\ldots\ldots\ldots\ldots$ (23)

From this we obtain to first-order

$$\Delta u_n' = \Delta u_n + \frac{(1-\phi)\, \rho_R (\partial u_R / \partial \rho_n)_{u_n} (R_n \Delta u_n - \rho_n)}{\phi(\rho_n + \Delta \rho_n) + (1-\phi) \rho_R (\partial u_R / \partial u_n)_{\rho_n}} .$$

$\ldots\ldots\ldots\ldots\ldots\ldots$ (24)

During phase transitions the derivatives in Eq. 24 undergo a finite jump. To ensure a high accuracy in the calculation, fluid energy changes during rock/fluid equilibration are computed twice, with

derivatives taken both: (1) forward, and (2) backward in time (see Figs. 2 and 3). Time steps are chosen such as to guarantee an absolute error smaller than some preset value.

Equation of State

Before each time step and for each volume element, we need to compute a number of parameters as functions of fluid energy and density (see Table 1). The calculational effort involved in this process can be quite substantial. SHAFT78 uses a method that is both flexible and efficient. We tabulate the parameters given in Table 1 as functions of u and ρ over a rectangular grid (u_n, ρ_m) (n = 1, ..., N; m = 1, ..., M). Parameters for the desired values of (u, ρ) then are "looked up" through bivariate interpolation. Special provisions are made (1) to avoid interpolating across the saturation line, at which parameters change slope; and (2) to tabulate the liquid region (subcooled water), which is very much compressed in an (u, ρ)-diagram.

The tabulation of fluid properties as functions of (u, ρ) is handled by two preprocessor programs. The first of these computes the analytical steam table equations, as given by the International Formulation Committee,[12] whereas the second inverts these tables into functions of (u, ρ), and appends parameters other than T,p,S.

3. RESULTS OF CALCULATION

Details of the choice of parameters and time steps in the calculations to be presented below can be found in Ref. 26.

Verification of SHAFT78

We have made careful checks of the accuracy of the various components of SHAFT78, as well as of the program as a whole. Typical accuracies obtained in interpolating the equation of state for water from given values of energy and density are better than 0.1% for temperatures, better than 0.2% for pressures, and about 0.01% for vapor saturations. An exception to this are pressures for subcooled water, which have an inaccuracy of typically $\pm$ 0.5 bars due to the extremely small compressibility of liquid water.

Calculations for one-dimensional gas flow and for radial flow to a line source in subcooled liquid water were made and found to agree well with analytical solutions published in the literature.[19-21] These examples involve little energy flow and check only the algorithm for solving the density Eq. 9 and the flow terms in Eq. 11.

In order to check both energy and density equations as well as the rock/fluid equilibration, we performed a number of two-phase calculations. The first example involves production from a two-dimensional aerial reservoir with an initial liquid saturation of 20%. This system was investigated initially by Toronyi and Farouq Ali, with their calculation subsequently verified by other workers.[3,5] A complete specification of the problem can be found in these references. Table 2 compares our results for liquid saturation after producing 19% of the reservoir fluid with those computed by Toronyi. The discrepancies are of the order of 1% and probably can be attributed to different weighting procedures.

A more severe test is afforded by a radial production problem as investigated by Garg.[22] The problem, which is defined in Table 3, involves withdrawal from a reservoir initially filled with subcooled water. As production proceeds, water begins to boil and several elements cross the saturation line. Fig. 4 shows that our calculation agrees well with the results obtained by Garg.

Total Kinematic Mobility

It was recently discovered by Garg that for a line source problem the equations governing two-phase flow can be approximately reduced to a single diffusion equation for pressure.[22] This equation holds for "early" times (production or injection small compared with fluid mass in place) near the wellbore. It admits an analytical solution, according to which pressure decline at the wellbore is approximately a linear function of log (time), with the slope inversely proportional to the "total kinematic mobility,"

$$\left(\frac{k}{\nu}\right)_T = \frac{k\, k_\ell \rho_\ell}{\mu_\ell} + \frac{k\, k_v \rho_v}{\mu_v} \quad \ldots\ldots\ldots \quad (25)$$

We have performed calculations for different saturations and different relative and absolute permeabilities, the results of which confirm Garg's theory. Fig. 5a shows, as an example, a pressure drawdown in a reservoir with an absolute permeability of 10^{-13} m^2 (100 md) and an initial saturation of 50%, with relative permeabilities as given in Ref. 27. (All other parameters are identical to those given in Table 3.) p vs log (time) is indeed a linear function, and from the slope we find $(k/\nu)_T$ = 1.16 x 10^{-7} sec to be compared with an average value of $(k/\nu)_T$ = 1.14 x 10^{-7} sec computed from Eq. 25. In Fig. 5b we have plotted p vs $\log(t/r^2)$ for the same simulation, but including <u>all</u> elements, not just the wellblock. Again a straight line results, with slope almost identical to that of Fig. 5a. This result, which is outside the scope of Garg's theory, seems to indicate that total kinematic mobilities also could be obtained from observation well data rather than just from flowing wellbore data.

Pressure Drawdown in Two-Phase Reservoirs

Two-phase reservoirs are capable of a great variety of pressure responses for constant-rate production,* depending mainly on (1) the initial amount and distribution of pore water, (2) residual immobile water saturation, and (3) rock porosity and permeability. An example of more unusual pressure drawdowns is given in Fig. 6. The simulation shown in Fig. 6 is for a reservoir that was investigated some time ago using a lumped parameter formulation by Brigham and Morrow.[23] The system is defined in Table 4. Our results differ greatly

*We investigate constant rate production at present rather than a practically more realistic constant pressure boundary condition for the well. The reason is that for the former we can obtain approximate analytical solutions with which to compare our simulation calculations.

from those of Ref. 23, the main reason being that the drawdown is dominated by mobility effects that are not accounted for by a lumped parameter formulation. (Besides this, the results of Ref. 23 appear to have an error in the energy balance, as temperatures and pressures drop far below the limiting values corresponding to evaporation of all pore water.)

The mechanism leading to the curious pressure drawdowns, as exhibited in Fig. 6, is interesting and warrants a more detailed discussion. Initially, pressure decline is governed by depletion of the steam above the water table. After a while the pressure drop reaches the water table, at which time water begins flowing upward and flashes into the steam zone. This causes a temperature drop near the bottom of the steam zone such that soon a small two-phase region develops above the water table. The flow of water also causes a pressure drop below the water table, which gives rise to in-situ boiling and an upward movement of water from below the water table. Because liquid water transmits pressure decline very rapidly, the pressure drop spreads quickly below the water table, distributing the rock heat loss in the subsequent boiling over a large volume. Thus, two boiling fronts emerge from the initial water/steam interface: The upward moving front moves slowly and has a relatively low temperature, whereas the downward moving front moves quickly and remains close to the initial rock temperature. After a while the steam saturation in the lower boiling region is large enough for significant quantities of steam to flow upward. This steam increases the temperatures and pressures at the two-phase front above the water table, giving rise to a slowing in pressure decline or even an increase in average reservoir steam pressure as well as steam pressure in the wellblock. The phenomenon depends critically on the value of the residual immobile water saturation, S_{res}, and on absolute and relative permeabilities in the steam and water regions. If S_{res} is decreased, the flash front initially will move more readily upward above the water table, causing less initial decline of temperature and pressure. Increasing the absolute permeability in the liquid region (in comparison with the steam region) accelerates the downward moving two-phase front relative to the upward moving one. Then initial pressure decline is enhanced, but pressure recovery is more pronounced once the entire liquid region is boiling. This is the reason for the (local) maximum in one of the curves in Fig. 6.

For the reservoir of Table 4 with a uniform initial steam saturation of S = 0.5, we obtain results qualitatively similar to those of Brigham and Morrow (except that their pressure and temperature declines are too large in absolute magnitude presumably due to numerical error). Fig. 7 gives the drawdown histories for three reservoirs that are identical except that the rock porosity is 5%, 10%, and 20%, respectively. Thus, the initial masses of fluid in place differ by a factor of 2 between reservoirs. Pressure drawdowns are virtually the same for these reservoirs for a considerable length of time. Obviously, pressure decline curves cannot be used for reserve assessment. Note that after the pore water is depleted, pressure falls to zero rapidly, because of rapid depletion of an all-steam phase. The standard technique of inferring reserves from pressure decline curves in (one-phase) gas or steam reservoirs is based on the fact that pressure is proportional to density (when corrections are made for real-gas behavior). In a two-phase geothermal reservoir, however, pressure is a function of temperature alone, with density being an independent variable. The mass of fluid in place depends on density, not on pressure. Pressure and temperature decline because of the heat loss of the rock to the boiling water. For reservoirs with small spatial variations in parameters, average pressure decline depends only on the total amount of water evaporated. This simple fact appears to have been overlooked in the literature. In Refs. 23 and 3, pressure is plotted as a function of mass fraction produced, which results in different decline curves for different porosities. However, if pressure were plotted as function of total mass produced, the curves for different porosities would very nearly coincide. The initial close coincidence of pressure decline curves for the three reservoirs shown in Fig. 7 is due to the fact that the rate at which water boils is virtually the same for all, being approximately equal to the rate of steam production.

If rock volumetric heat capacity and initial average reservoir temperature are known, pressure decline curves can be used to estimate the total volume of a two-phase reservoir, as we shall show presently. Only if this information is supplemented by values for average porosity and average saturation can reserve estimates be made.

Reservoirs with small spatial variations in fluid and rock properties can be analyzed with the bulk model developed in the Appendix. Eq. A-13 shows that pressure drawdown at early times is a linear function of produced mass (we assume that liquid water is immobile at the well and only steam is produced). The slope of p(t) is inversely proportional to the reservoir volume (cf. Eq. A-13):

$$V(1-\phi) = -\frac{1}{\dot{p}} \frac{M}{\rho_R C_R} \left[\frac{\rho_v (h_v - h_\ell)^2}{T + 273.15}\right]_{t_o} \quad . . . \quad (26)$$

For the three reservoirs calculated in Fig. 7, the slopes are virtually the same. Inserting this value into Eq. 26 we obtain an estimate for the reservoir rock volume,

$$V(1-\phi) = 9.4 \times 10^8 \text{ m}^3. \quad . . . . . \quad (27)$$

This compares with values of 9.5, 9. and 8. x 10^8 m^3 for the three cases investigated.

Field observation of an initially linear dependence of pressure on time such as in Fig. 7 might be taken erroneously as an indication that the reservoir contains pure steam.[24,28] if the standard technique for estimating gas or steam reserves from a straight-line extrapolation then were used, large errors would be committed. A correct reserve estimate would be purely coincidental. This statement can be made more quantitative. Using Eq. A-13 we obtain for the ratio of mass reserves as estimated from a p/Z vs t-plot to true reserves ($\phi V \rho$),

$$\omega = \frac{1-\phi}{\phi} \frac{p\, \rho_R C_R (T + 273.15)}{\rho_v \rho_\ell (h_v - h_\ell)^2 [1 - (1-\rho_v/\rho_\ell)\, S]} \, . \quad . . . . . \quad (28)$$

All parameters are to be evaluated at the initial reservoir temperature and pressure. Values of ω for the reservoir of Table 4 (S = 0.5) are given in Table 5 for a range of porosities and saturations. Note that the p/Z-technique overestimates reserves for small porosity by large factors, especially when the vapor saturation is large. On the other hand, for large porosities and small saturations reserves are underestimated.

CONCLUSION

The simulator SHAFT78 has been verified for a number of one- and two-phase flow problems involving subcooled water, water/steam mixtures, and superheated steam. The flow of water and steam in porous media, boiling and condensation phenomena, and heat exchange between rock and fluid are all described properly.

A completely self-consistent iterative treatment of mass and energy flow currently is being implemented to overcome existing limitations of permissible size of time steps.

Model simulations revealed that two-phase geothermal reservoirs are capable of a large variety of pressure responses during fluid production. The main factor that determines pressure decline is the amount and distribution of pore water in the reservoir. Two-phase geothermal reservoirs often will exhibit a linear dependence of p/Z on cumulative production, similar to that observed in gas reservoirs. However, the standard gas reservoir technique of predicting reserves from the slope of p/Z vs cumulative production is not applicable for two-phase geothermal reservoirs, except under fortuitous circumstances. Reserve assessment requires knowledge of average porosity and vapor saturation, which cannot be obtained from pressure decline curves.

Apart from idealized model studies, SHAFT78 also has been used for a three-dimensional simulation of production and recharge in the Krafla geothermal field (Iceland), which is reported elsewhere.[13] At present, a history match for production and injection in the Serrazzano field (Italy) is being developed.[14]

NOMENCLATURE

A_{nm} = interface area between volume elements n and m, m^2
a = general element of area, m^2
C_R = specific heat of rock, J/°C kg
d_n, d_m = distance of interface from center of volume elements, m
$\underset{\sim}{F}$ = mass flux, kg/m^2s
$\underset{\sim}{F}_\ell$ = flux of liquid, kg/m^2s
$\underset{\sim}{F}_v$ = flux of vapor, kg/m^2s
F_{nm} = mass flux between volume elements n, m, kg/m^2s
$\underset{\sim}{G}$ = energy flux, J/m^2s
G_{nm} = energy flux between volume elements n, m, J/m^2s
$\underset{\sim}{g}$ = vector of gravitational acceleration, m/s^2
g_{nm} = component of gravitational acceleration perpendicular to the interface between volume elements n, m, m/s^2
h = specific enthalpy of fluid, J/kg
h_ℓ = specific enthalpy of liquid, J/kg
h_v = specific enthalpy of vapor, J/kg
h_R = specific enthalpy of rock, J/kg
I = integrand of pressure equation, ms^2 °C/J
K = thermal conductivity of rock/fluid mixture, J/ms °C
K_n, K_m = average thermal conductivity in volume elements n, m, J/ms °C
K_{nm} = average thermal conductivity at interface between volume elements n, m, J/ms°C
K_R = thermal conductivity of rock, J/ms°C
k = absolute permeability, m^2
k_n, k_m = average absolute permeability in volume elements n, m, m^2
k_{nm} = absolute permeability at interface between volume elements n, m, m^2
k_ℓ = relative permeability of liquid, fraction
k_v = relative permeability of vapor, fraction
$(k/\nu)_T$ = total kinematic mobility, s
$\dot{M}$ = rate of fluid production, kg/s
$\underset{\sim}{n}$ = unit normal on aerial element
$\underset{\sim}{p}$ = pressure, N/m^2
p_n, p_m = average pressure in volume elements n, m, N/m^2
p_o = pressure at initial time, N/m^2
$\dot{p}$ = slope of pressure vs time, N/m^2s
q = volumetric rate of mass generation, kg/m^3s
q_n = average volumetric rate of mass generation in volume element n, kg/m^3s
Q = volumetric rate of energy generation, J/m^3s
Q_n = average volumetric rate of energy generation in volume element n, J/m^3s
R = ratio of density to energy change, $(kg/m^3)/(J/kg)$
R_n = average ratio of density to energy change in volume element n, $(kg/m^3)/(J/kg)$
r_i = radial length of volume element i of radial grid, m
S = volumetric vapor saturation, fraction
S_{res} = residual immobile volumetric liquid saturation, fraction
T = temperature, °C
T_n, T_m = average temperature in volume elements n, m, °C
t = time, s
t_u = time step for energy equation, s
t_ρ = time step for density equation, s
t_o = initial time, s
u = specific energy of fluid, J/kg
u_n, u_m = average specific energy of fluid in volume elements n, m, J/kg
u_{nm} = average specific energy of fluid at interface between volume elements n, m, J/kg
u_ℓ = specific energy of liquid, J/kg
u_v = specific energy of vapor, J/kg
u_R = specific energy of rock, J/kg
u_{up} = average specific energy of upstream volume element, J/kg
u_{down} = average specific energy of downstream volume element, J/kg

V = volume of reservoir, m^3

V_n, V_m = volume elements of reservoir, m^3

(V_n) = surface of volume element V_n, m^2

Z = gas law compressibility factor, dimensionless

Δ = increment

$\mathcal{E}$ = fluid energy per volume, J/m^3

κ = weighting factor for mobilities, dimensionless

λ = weighting factor for energies, dimensionless

ρ = fluid density, kg/m^3

ρ_n, ρ_m = average fluid density in volume elements n, m, kg/m^3

ρ_{nm} = average fluid density at interface between volume elements n, m, kg/m^3

ρ_o = initial fluid density, kg/m^3

ρ_ℓ = density of liquid, kg/m^3

ρ_v = density of vapor, kg/m^3

ρ_α = density of phase α, kg/m^3

ρ_R = density of rock, kg/m^3

τ = general volume element, m^3

θ = time weighting factor, dimensionless

μ_ℓ = viscosity of liquid, Ns/m^2

μ_v = viscosity of vapor, Ns/m^2

μ_α = viscosity of phase α, Ns/m^2

ϕ = porosity, dimensionless

ϕ_n = porosity of volume element n, dimensionless

ω = ratio of (p/Z)—estimate to true reserves, dimensionless

Subscripts

down = downstream

exp = explicit

ℓ = liquid

n, m = volume elements

R = rock

res = residual

ρ = referring to density

u = referring to energy

up = upstream

v = vapor

α = liquid or vapor phase

REFERENCES

1. White, D. E., Muffler, L.J.P., and Truesdell, A. H.: "Vapor-Dominated Hydrothermal Systems Compared with Hot-Water Systems," Econ. Geology (1971) 66, 75-97.
2. Bird, R. B., Stewart, W. E., and Lightfoot, E. N.: Transport Phenomena, John Wiley & Sons, Inc., NY, London, Sydney (1960).
3. Toronyi, R. M. and Farouq Ali, S. M.: "Two-Phase, Two-Dimensional Simulation of a Geothermal Reservoir," Soc. Pet. Eng. J. (June 1977) 171-183.
4. Moench, A. F.: "Simulation of Steam Transport in Vapor-Dominated Geothermal Reservoirs," Report No. 76-607, USGS, Menlo Park, CA (1976).
5. Thomas, L. K. and Pierson, R. G.: "Three-Dimensional Geothermal Reservoir Simulation," Soc. Pet. Eng. J. (April 1978) 151-161.
6. Coats, K. H.: "Geothermal Reservoir Modeling," paper SPE 6892 presented at the SPE-AIME 52nd Annual Fall Technical Conference and Exhibition, Denver, Oct. 9-12, 1977.
7. Garg, S. K., Pritchett, J. W., Rice, M. H., and Riney, T. D.: "U.S. Gulf Coast Geopressured Geothermal Reservoir Simulation," Report SSS-R-77-3147, Systems, Science and Software, La Jolla, CA (1977).
8. Mercer, J. W. and Faust, C.: "Progress Report on Multiphase Geothermal Modeling," Proc., Third Stanford Workshop on Geothermal Reservoir Engineering, Stanford, CA (1977) 185-187.
9. Moench, A. F. and Atkinson, P. G.: "Transient Pressure Analysis in Geothermal Steam Reservoirs with an Immobile Vaporizing Liquid Phase — Summary Report," Proc., Third Stanford Workshop on Geothermal Reservoir Engineering, Stanford, CA (1977) 64-69.
10. Huyakorn, P. S., Pinder, G. F., Faust, C. R., and Mercer, J. W.: "Finite Element Simulation of Two-Phase Flows in Porous Media," preprint to be presented at the ASME Winter Annual Meeting (Dec. 1978).
11. Narasimhan, T. N. and Witherspoon, P. A.: "An Integrated Finite Difference Method for Analyzing Fluid Flow in Porous Media," Water Resources Research (Feb. 1976) 12, 57-64.
12. International Formulation Committee: "The 1967 IFC Formulation for Industrial Use, A Formulation of the Thermodynamic Properties of Ordinary Water Substance" (Feb. 1967).
13. Jonsson, V.: "Simulation of the Krafla Geothermal Field," Lawrence Berkeley Laboratory Rept. LBL-7076, Berkeley, CA (1978).
14. Weres, O.: "A Model of the Serrazzano Zone," Proc., Third Stanford Workshop on Geothermal Reservoir Engineering, Stanford, CA (1977) 214-219.
15. Hubbert, M. K.: "Darcy's Law and the Field Equations of the Flow of Underground Fluids," Trans., AIME (1956) 207, 222-239.
16. Evans, G. W., Brousseau, R. J., and Keirstead, R.: "Instability Considerations for Various Difference Equations Derived from the Diffusion Equation," Lawrence Livermore Lab. Rept. UCRL-4476, Livermore, CA (1954).
17. Lasseter, T. J., Witherspoon, P. A., and Lippmann, M. J.: "Multiphase Multidimensional Simulation of Geothermal Reservoirs," Proc., Second United Nations Symposium on the Development and Use of Geothermal Resources, San Francisco, CA (1975) 3, 1715-1723.
18. Peaceman, D. W.: Fundamentals of Numerical Reservoir Simulation, Elsevier Scientific Publ. Comp., Amsterdam, Oxford, NY (1977).
19. Kidder, R. E.: "Unsteady Flow of Gas Through A Semi-Infinite Porous Medium," J. Appl. Mech. (Sept. 1957) 329-332.
20. Matthews, C. S. and Russell, D. G.: Pressure Buildup and Flow Tests in Wells, Monograph Series, Society of Petroleum Engineers of AIME, Dallas (1967) 1, 13-16.
21. Pruess, K., Schroeder, R. C., and Zerzan, J. M.: "Studies of Flow Problems with the Simulator SHAFT78," paper to be presented at the Fourth Stanford Workshop on Geothermal Reservoir Engineering, Stanford, CA (Dec. 13-15, 1978).
22. Garg, S. K.: "Pressure Transient Analysis for Two-Phase (Liquid Water/Steam) Geothermal Reservoirs," paper SPE 7479 presented at the SPE-AIME 53rd Annual Fall Technical Conference and Exhibition, Houston, Oct. 1-3, 1978.
23. Brigham, W. E. and Morrow, W. B.: "p/Z Behavior for Geothermal Steam Reservoirs," Soc.

Pet. Eng. J. (Dec. 1977) 407-412.

24. Ramey, H. J., Jr.: "A Reservoir Engineering Study of the Geysers Geothermal Field," testimony for the trial of Reich and Reich vs Commissioner of the Internal Revenue, Tax Court of the U.S., 52, T. C. No. 74 (1970).
25. Van Wylen, G. J. and Sonntag, R. E.: Fundamentals of Classical Thermodynamics, John Wiley & Sons, Inc., New York (1973).
26. Pruess, K., Schroeder, R. C., Witherspoon, P. A., and Zerzan, J. M.: "SHAFT78, A Two-Phase Multidimensional Computer Program for Geothermal Reservoir Simulation," Lawrence Berkeley Lab. Rept. LBL-8264, Berkeley, CA (1978).
27. Muskat, M., Wyckoff, R. D., Bobset, H. G., and Meres, M. W.: "Flow of Gas-Liquid Mixtures Through Sands," Trans., AIME (1937) 123, 69.
28. Atkinson, P., Celati, R., Marconcini, R., Miller, F., and Neri, G.: "Analysis of Reservoir Pressures and Decline Curves in Serrazzano Zone, Larderello Geothermal Field," Proc., of the Larderello Workshop on Geothermal Resource Assessment and Reservoir Engineering, Larderello, Italy (Sept. 12-16, 1977) 208-232.

APPENDIX - BULK MODEL FOR TWO-PHASE RESERVOIR

Consider a two-phase reservoir with initial conditions and rock properties independent of position, and a constant volumetric rate of steam production, $q < 0$. For this system the mass and energy-balance equations (Eqs. 1 and 2) reduce to

$$\phi d\rho = q dt \quad \ldots\ldots\ldots\ldots\ldots\ldots \quad (A\text{-}1)$$

$$d\left(\frac{\text{energy}}{\text{volume}}\right) = q\, h_v\, dt \quad \ldots\ldots\ldots\ldots \quad (A\text{-}2)$$

with (energy/volume) given by Eq. 5. We have

$$d\left(\frac{\text{energy}}{\text{volume}}\right) = \phi d\varepsilon + (1-\phi)\,\rho_R C_R\, dT \quad \ldots \quad (A\text{-}3)$$

where we have introduced the specific volumetric energy $\varepsilon = u\rho$ of the fluid. The usefulness of formulating in terms of ε rather than u is that ε can be written explicitly in a way that separates the ρ- and T-dependence, namely,

$$\varepsilon = u\rho = \rho_\ell \rho_v \frac{u_v - u_\ell}{\rho_\ell - \rho_v} + \frac{u_\ell \rho_\ell - u_v \rho_v}{\rho_\ell - \rho_v}\,\rho \,.$$

$$\ldots\ldots\ldots\ldots\ldots\ldots\ldots \quad (A\text{-}4)$$

All quantities except ρ depend on T only. From Eqs. A-1 through A-4 follows

$$d\rho = (1 - \rho_v/\rho_\ell)\,\frac{\frac{1-\phi}{\phi}\,\rho_R C_R + \left(\frac{\partial \varepsilon}{\partial T}\right)_\rho}{h_v - h_\ell}\, dT \,.$$

$$\ldots\ldots\ldots\ldots\ldots\ldots\ldots \quad (A\text{-}5)$$

The only term on the right-hand side that depends on ρ is $(\partial\varepsilon/\partial T)_\rho$, i.e., the volumetric specific heat of the (two-phase) fluid at constant density. In all practical cases, with porosity considerably less than 1, this will be negligible in comparison with the rock contribution $(1-\phi)\,\rho_R C_R/\phi$. Neglecting $(\partial\varepsilon/\partial T)_\rho$, we achieve a separation of variables in Eq. A-5, which admits a closed-form solution,

$$\rho - \rho_o = \frac{1-\phi}{\phi}\,\rho_R C_R \int_{\rho_o}^{\rho} (1-\rho_v/\rho_\ell)\,\frac{dT}{h_v - h_\ell} \,.$$

$$\ldots\ldots\ldots\ldots\ldots\ldots\ldots \quad (A\text{-}6)$$

To obtain the pressure drawdown with time, we use Eq. A-1 to write ρ as function of time, and express T as a function of p:

$$dT = \left(\frac{dT}{dp}\right)_{sat} dp = \frac{(\rho_\ell - \rho_v)(T + 273.15)}{\rho_\ell \rho_v\,(h_v - h_\ell)}\, dp \,.$$

$$\ldots\ldots\ldots\ldots\ldots\ldots\ldots \quad (A\text{-}7)$$

Away from the critical point we may neglect $\rho_v/\rho_\ell \ll 1$, so that

$$t - t_o = \frac{1}{q}\,(1-\phi)\,\rho_R C_R \int_{t_o}^{t} \frac{(T + 273.15)}{\rho_v (h_v - h_\ell)^2}\, dp \,.$$

$$\ldots\ldots\ldots\ldots\ldots\ldots\ldots \quad (A\text{-}8)$$

This formula gives the pressure drawdown as an implicit function of time. To invert it to explicit form, we expand the integrand to first order. Abbreviating

$$I(p) = \frac{(T(p) + 273.15)}{\rho_v (h_v - h_\ell)^2} \quad , \ldots\ldots\ldots \quad (A\text{-}9)$$

we have

$$I(p) = I(p_o) + \left(\frac{dI}{dp}\right)_{p_o} (p - p_o) \quad \ldots\ldots (A\text{-}10)$$

from which, after performing the integration,

$$p(t) = p_o - \frac{1}{(d\ell nI/dp)_{p_o}} - \sqrt{\frac{2q(t - t_o)}{(1-\phi)\rho_R C_R (dI/dp)_{p_o}} + \frac{1}{(d\ell nI/dp)^2_{p_o}}}$$

$$\ldots\ldots\ldots\ldots\ldots\ldots\ldots\ldots (A\text{-}11)$$

(Note that $d\ell nI/dp < 0$).

At early times, defined by

$$t - t_o \ll \frac{(1-\phi)\,\rho_R C_R\,(dI/dp)_{p_o}}{2q\,(d\ell nI/dp)^2_{p_o}} \quad , \ldots (A\text{-}12)$$

we can expand the square root and obtain a linear pressure drawdown:

$$p(t) = p_o - \frac{|q|}{(1-\phi)\rho_R C_R} \left[\frac{\rho_v (h_v - h_\ell)^2}{(T + 273.15)}\right]_{t_o} (t - t_o) \,.$$

$$\ldots\ldots\ldots\ldots\ldots\ldots\ldots (A\text{-}13)$$

Table 1

Fluid parameters

Parameter	Meaning	Units
T	temperature	^{o}C
p	pressure	$N/m^2 = Pa$
S	vapor saturation	[volumetric fraction]
K	heat conductivity	$J/ms\ ^{o}C$
k_ℓ/μ_ℓ	rel. permeability/ viscosity for liquid	m^2/Ns
k_v/μ_v	rel. permeability/ viscosity for vapor	m^2/Ns
ρ_ℓ	density of liquid	kg/m^3
ρ_v	density of vapor	kg/m^3
u_ℓ	energy of liquid	J/kg
u_v	energy of vapor	J/kg

Table 2

Percentage of Liquid Water Saturations for Toronyi's Problem[a)]

1 18.3 18.3	2 17.2 17.3	3 15.2 15.2	4 12.2 11.8	5 14.8 14.9	6 16.2 16.4
7 18.3 18.3	8 17.2 17.3	9 15.2 15.2	10 12.2 11.7	11 14.8 14.9	12 16.2 16.4
13 18.3 18.3	14 17.2 17.3	15 15.2 15.2	16 12.1 11.8	17 14.8 14.9	18 16.2 16.4
19 18.3 18.3	20 17.2 17.3	21 15.2 15.2	22 12.2 11.8	23 14.8 14.9	24 16.2 16.4
25 18.3 18.3	26 17.2 17.3	27 15.2 15.2	28 12.3 12.0	29 14.8 14.9	30 16.2 16.4
31 18.3 18.3	32 17.2 17.3	33 15.2 15.2	34 12.3 12.0	35 14.8 14.9	36 16.2 16.4

a) The lower numbers are Toronyi's results, whereas the upper ones were computed from SHAFT78.

Table 3

Garg's Problem

Rock properties: $\rho_R = 2.65 \times 10^3$ kg/m^3
$C_R = 1$ kJ/kg
$K_R = 5.25$ W/m$^\circ$C
$k = 10^{-14}$ m^2
$\phi = 20\%$

Reservoir geometry: The reservoir is a 5.625°-sector of a cylindrically symmetrical reservoir, subdivided into 50 elements with radial increments as follows:

$$\Delta r_1 = \Delta r_2 = \ldots = \Delta r_{11} = 1 \text{ m}; \ \Delta r_{12} = 1.2\ \Delta r_{11},$$

$$\Delta r_{13} = 1.2\ \Delta r_{12} \ldots \Delta r_{50} = 1.2\ \Delta r_{49}.$$

Mass is withdrawn from element 1 at a rate of .14 kg/s·m

The boundary conditions at the outer sector are "no flow."

Initial conditions are $T = 300\ ^\circ$C, $p = 90$ bars for the simulation shown in Figure 4, and $T = 300\ ^\circ$C, $S = 50\%$ for the simulation shown in Figure 5a,b.

Table 4

Brigham/Morrow Problem

Rock properties: $\rho_R = 2000$ kg/m^3
$C_R = 1232$ J/kg
$K_R = 0.$
$k = 10^{-13}$ m^2
$\phi = 5, 10, 20\%$

The reservoir is a cube with 1 km^3 volume. For the case studied in Figure 7 it was subdivided into 10 equal-sized elements with a vertical spacing of 100 m. For the problem of Figure 6 the top 3 and bottom 2 elements have a vertical spacing of 100 m, with the 500 m between them divided into 20 equal-sized elements of 25 m vertical separation. All outer boundaries are "no flow." Mass is withdrawn at the top at a rate of 50 kg/s. Initial conditions are:

	T	p	S	elements
Figure 6	252 $^\circ$C	41 bars	1.0	top 500 m
	252 $^\circ$C	41.1 bars	0.001	bottom 500 m
Figure 7	252 $^\circ$C	41.1 bars	0.5	all

Table 5

Ratio of (p/z) - Estimates to True Reserves in a Two-Phase Reservoir

values of ω[a]						
S \ ϕ	.01	.02	.05	.10	.20	.30
.05	11.6	5.7	2.2	1.1	.47	.27
.10	12.2	6.0	2.3	1.1	.49	.29
.20	13.7	6.8	2.6	1.2	.55	.32
.30	15.5	7.7	3.0	1.4	.63	.37
.40	18.0	8.9	3.5	1.6	.73	.42
.50	21.4	10.6	4.1	1.9	.87	.51
.60	26.5	13.1	5.1	2.4	1.1	.62
.70	34.5	17.1	6.6	3.1	1.4	.81
.80	49.8	24.6	9.6	4.5	2.0	1.2
.90	89.1	44.1	17.1	8.1	3.6	2.1
.95	147.	72.8	28.2	13.4	5.9	3.5

[a] The table is computed from eq. (28). It shows the factors ω by which application of the p/Z vs. t-method would overestimate mass reserves for the reservoir of Table 4 (initial temperature: $T = 252^{\circ}C$). The same general pattern with somewhat different numerical values holds for different rock parameters and initial temperatures.

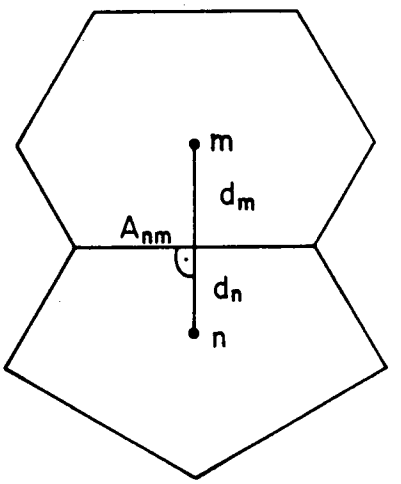

XBL7811-12743

FIG. 1 - ILLUSTRATION OF ELEMENTS, INTERFACES, AND DISTANCES. ELEMENTS N AND M ARE SHOWN AS TWO-DIMENSIONAL POLYGONS WITH INTERFACE AREA A_{NM} AND ELEMENT CENTERS BEING AT A DISTANCE D_N AND D_M, RESPECTIVELY, FROM THE INTERFACE.

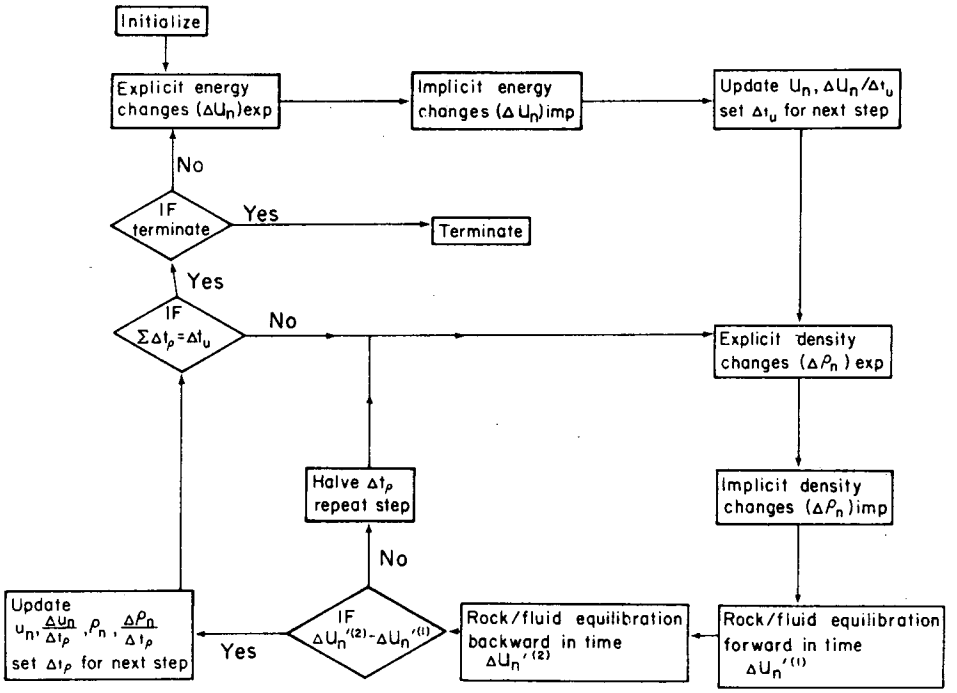

FIG. 2 - FLOW CHART OF PROGRAM EXECUTION. (FOR AN EXPLANATION SEE TEXT.) XBL7811-12742

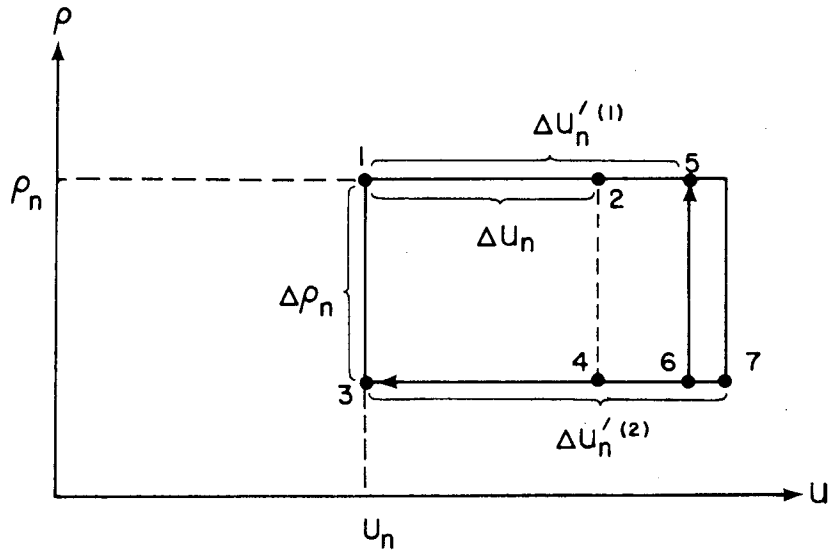

XBL7811-12744

FIG. 3 - ROCK/FLUID EQUILIBRATION. LET ELEMENT N BE AT (U_N, ρ_N) AT THE BEGINNING OF TIME STEP T^K (POINT 1). SOLVING ENERGY AND DENSITY EQUATIONS IT WILL MOVE TO $(U_N + \Delta U_N, \rho_N + \Delta \rho_N)$ (POINT 4). THE ROCK/FLUID EQUILIBRATION WITH DERIVATIVES AVERAGED OVER 1-2 AND 1-3, RESPECTIVELY (SEE EQ. 24), WILL GIVE $(U_N + \Delta U_N'^{(1)}, \rho_N + \Delta \rho_N)$(POINT 6). REPEATING ROCK/FLUID EQUILIBRATION WITH DERIVATIVES AVERAGED OVER 6-5 AND 6-3, RESPECTIVELY, WILL GIVE $(U_N + \Delta U_N'(2)$, $\rho_N + \Delta \rho_N)$(POINT 7). IF $\Delta U_N'(1)$ AND $\Delta U_N'(2)$ DIFFER BY MORE THAN A PRESCRIBED AMOUNT, THE DENSITY STEP IS REPEATED WITH HALF THE TIME INCREMENT. LARGE RELATIVE CHANGES IN $\Delta U_N'$ OCCUR IF THE SATURATION LINE WAS CROSSED (POINTS 1 AND 6 BEING ON OPPOSITE SIDES OF THE SATURATION LINE). THEN SMALL TIME STEPS ARE TAKEN WITH SMALL ABSOLUTE ERRORS UPON CROSSING THE SATURATION LINE.

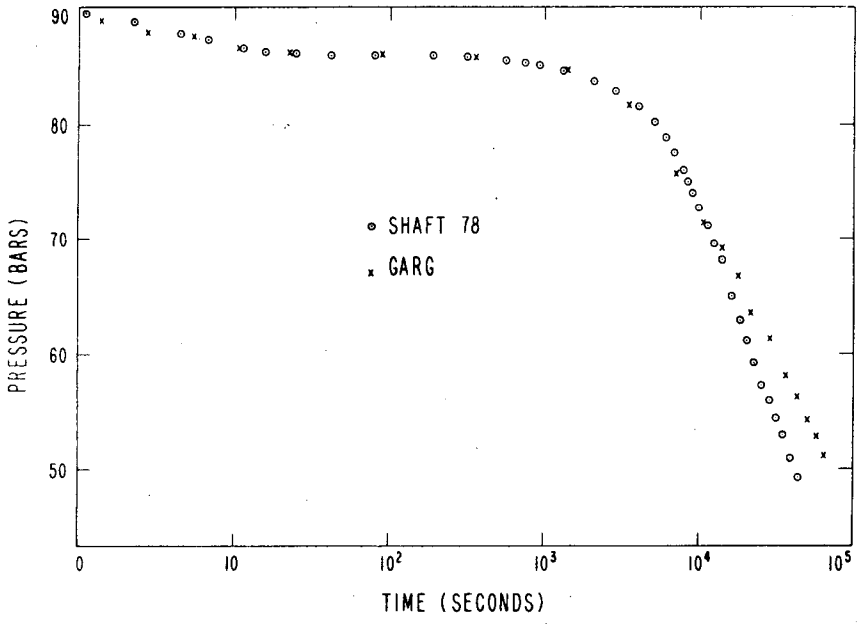

XBL 7811-2168

FIG. 4 - SIMULATED PRESSURE DRAWDOWN FOR RADIAL WATER RESERVOIR. THE RELATIVE PERMEABILITIES ARE TAKEN FROM COREY'S EQUATION, WITH $S_{GC} + S_{WC} = .35$. THE OTHER PARAMETERS OF THE PROBLEM ARE DEFINED IN TABLE 3. THE RESULTS OF THE SHAFT78-SIMULATION (CIRCLES) COMPARE WELL WITH GARG'S RESULTS (CROSSES).

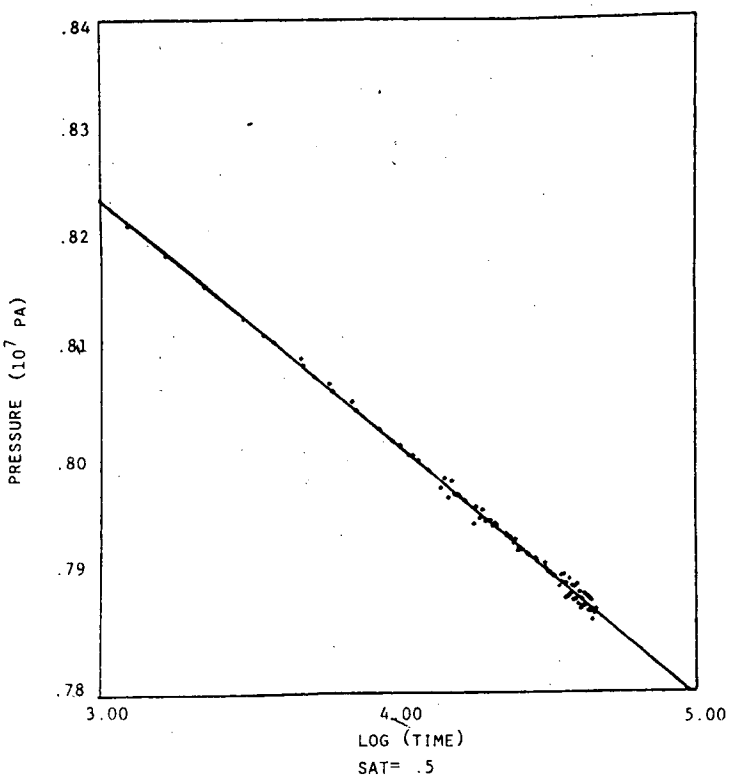

XBL 7811-13174

FIG. 5A - SIMULATED PRESSURE DRAWDOWN FOR A RADIAL TWO-PHASE RESERVOIR. THE PROBLEM IS SPECIFIED IN TABLE 4, EXCEPT THAT K = 100 MILLIDARCY (10^{-13} M^2). RELATIVE PERMEABILITIES USED WERE THOSE OF REF. 27.

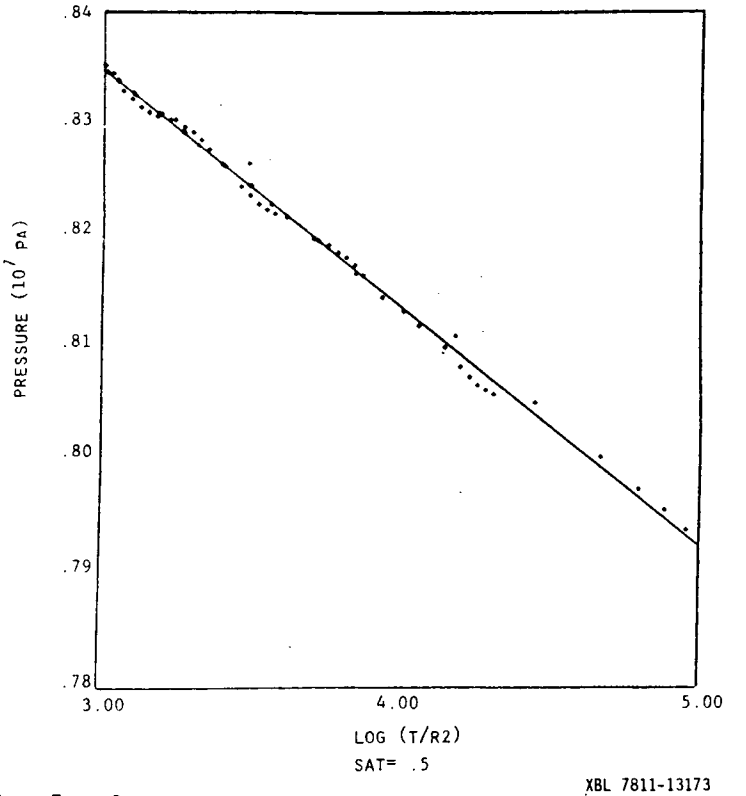

XBL 7811-13173

FIG. 5B - SIMULATED PRESSURE DRAWDOWN FOR A RADIAL TWO-PHASE RESERVOIR. THE PROBLEM IS SPECIFIED IN TABLE 4, EXCEPT THAT K = 100 MILLIDARCY (10^{-13} M^2). RELATIVE PERMEABILITIES USED WERE THOSE OF REF. 27.

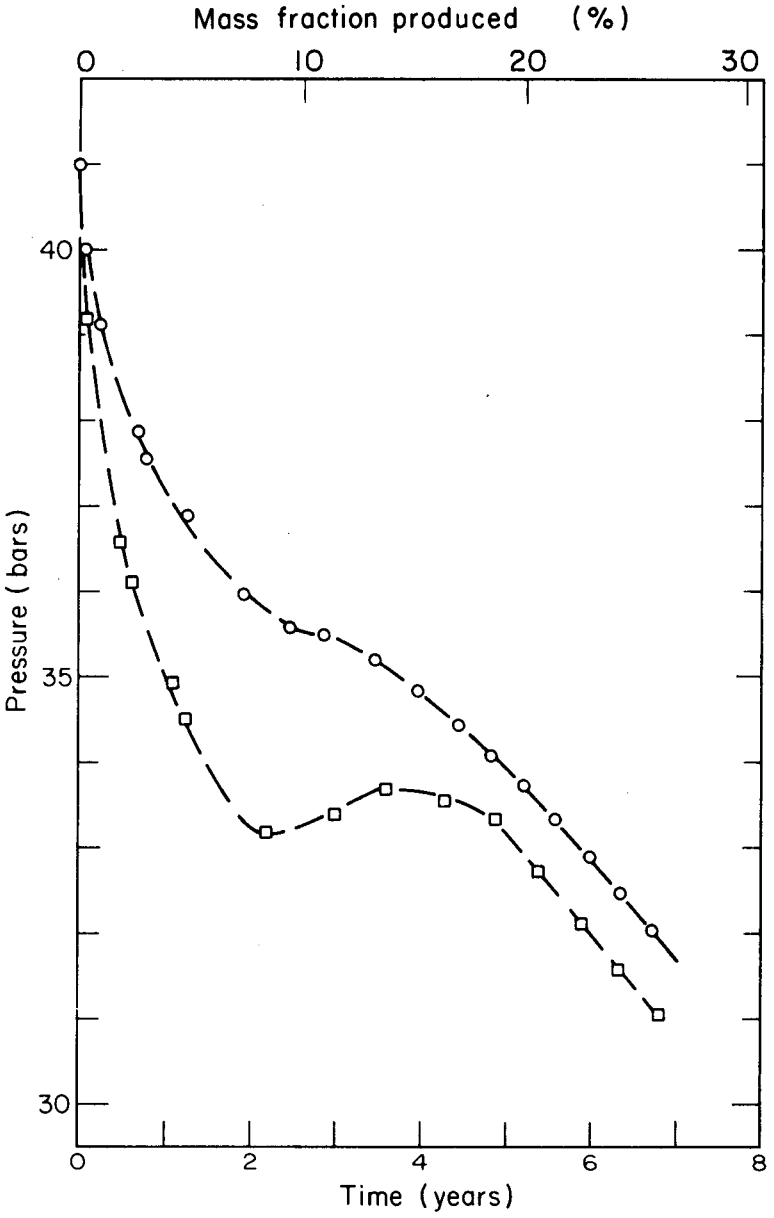

XBL 7811-12720

Fig. 6 - Simulated pressure drawdowns in a one-dimensional two-phase reservoir with a water/steam interface. The relative permeabilities were obtained from Corey's equation as given in ref. 5, with $S_{gc} + S_{wc} + 7$. The circles are for a simulation as specified in Table 4, with porosity ϕ = 10%. The rectangles are for the same system but the bottom 500 m have been taken to be one element; this corresponds to a very large absolute permeability in this region.

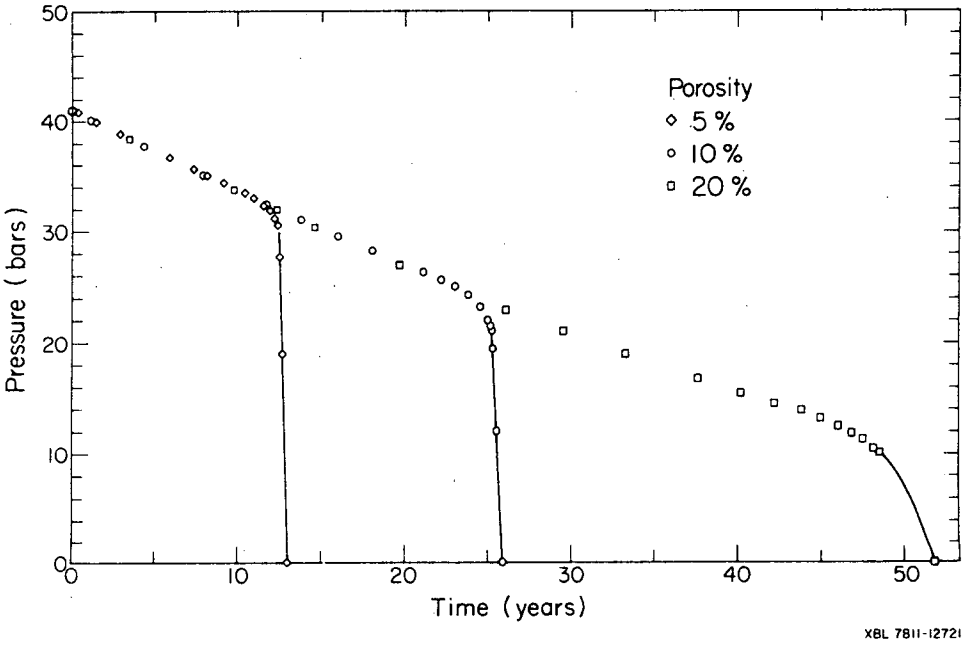

FIG. 7 - SIMULATED PRESSURE DRAWDOWN IN ONE-DIMENSIONAL TWO-PHASE RESERVOIRS WITH UNIFORM INITIAL SATURATION. THE PROBLEM IN DEFINED IN TABLE 4.

This report was done with support from the Department of Energy. Any conclusions or opinions expressed in this report represent solely those of the author(s) and not necessarily those of The Regents of the University of California, the Lawrence Berkeley Laboratory or the Department of Energy.

TECHNICAL INFORMATION DEPARTMENT
LAWRENCE BERKELEY LABORATORY
UNIVERSITY OF CALIFORNIA
BERKELEY, CALIFORNIA 94720